Free Convection of Hybrid Nanofluids in a C-Shaped Chamber under Variable Heat Flux and Magnetic Field: Simulation, Sensitivity Analysis, and Artificial Neural Networks

Hamed Bagheri [1], Mohammadali Behrang [1,2], Ehsanolah Assareh [1], Mohsen Izadi [3] and **Mikhail A. Sheremet [4,*]**

[1] Department of Mechanical Engineering, Dezful Branch, Islamic Azad University, Dezful 61424-20890, Iran
[2] Farab Power Generation & Operation Management Co., Tehran 15946-59914, Iran
[3] Mechanical Engineering Department, Faculty of Engineering, Lorestan University, Khorramabad 68151-44316, Iran
[4] Laboratory on Convective Heat and Mass Transfer, Tomsk State University, Tomsk 634050, Russia
[*] Correspondence: sheremet@math.tsu.ru

Abstract: In the present investigation, the free convection energy transport was studied in a C-shaped tilted chamber with the inclination angle α that was filled with the MWCNT (MultiWall Carbon Nanotubes)-Fe_3O_4-H_2O hybrid nanofluid and it is affected by the magnetic field and thermal flux. The control equations were numerically resolved by the finite element method (FEM). Then, using the artificial neural network (ANN) combined with the particles swarm optimization algorithm (PSO), the Nusselt number was predicted, followed by investigating the effect of parameters including the Rayleigh number (Ra), the Hartmann number (Ha), the nanoparticles concentration (φ), the inclination angle of the chamber (α), and the aspect ratio (AR) on the heat transfer rate. The results showed the high accuracy of the ANN optimized by the PSO algorithm in the prediction of the Nusselt number such that the mean squared error in the ANN model is 0.35, while in the ANN model, it was optimized using the PSO algorithm (ANN-PSO) is 0.22, suggesting the higher accuracy of the latter. It was also found that, among the studied parameters with an effect on the heat transfer rate, the Rayleigh number and aspect ratio have the greatest impact on the thermal transmission intensification. The obtained data also showed that a growth of the Hartmann number illustrates a reduction of the Nusselt number for high Rayleigh numbers and the heat transfer rate is almost constant for low Rayleigh number values.

Keywords: heat transfer; hybrid nanofluid; Nusselt number; artificial neural network; particles swarm algorithm

1. Introduction

Particles with micrometer size were traditionally added to fluids to increase their thermal conductivity coefficient. However, these particles did not have the required stability in the suspension and was quickly deposited, leading to the blockage of the fluid passageway. In comparison, nano-sized particles form a much more stable suspension and the problem of channel chocking and blocking is minimized due to lower sedimentation rates. Generally, nanoparticles are produced for the size range of 1 nm to 100 nm, depending on the type of operation. Nanoparticles can play a significant role in improving the environment and reducing environmental pollutants. Nanofluids were first prepared by Choi in 1995 [1]. Since then, they have been considered by many researchers in engineering and

heat transfer applications owing to their improving heat transfer properties [2–17]. For the stable distribution of nanoparticles in the closed chambers, energy transport can be essentially improved compared to the absence of nanoparticles (i.e., base fluid only). It should be noted that nanofluids are used in different engineering applications such electronics cooling, solar collectors, heat exchangers, building insulation systems, and so on [18–20]. Khanafer et al. [21] are the first who numerically simulated the thermal transmission of the nanoliquid within the square-shaped chamber. They used the Wasp's and Brinkman correlations for thermal conductivity and viscosity, respectively. Their results indicated that the energy transport rises with a growth of the nanoparticles concentration. Ganvir et al. [22] presented a review article of previous studies about heat transfer properties of different nanofluids and concluded that, in all cases, the thermal conductivity of nanoliquids was more than the host liquid. Kalidasan and Rajesh [23] examined the use of nanofluids of multi-wall carbon nanotubes (MWCNTs) and water in increasing the natural convection within a closed chamber. They observed that thermal transmission can be intensified due to a growth of the Rayleigh number and concentration of nanotubes. Hasanuzzaman et al. [24] examined the influence of the magnetic field on thermogravitational convection inside a trapezoidal chamber. They sloped the walls of the chamber and fixed the temperature of the lower wall. Additionally, the upper wall was adiabatic and the temperature of the lower wall was considered to be greater than that of the steep wall. By examining the effects of various characteristics such as Rayleigh and Hartmann numbers, and angle of dip of the chamber wall on the energy transport, it was revealed that the thermal transmission decreases for various Rayleigh numbers by raising the nanoparticles concentration and magnetic field intensity. Sheremet et al. [25] investigated thermogravitational convection within a partially heated irregular chamber filled with porous medium saturated by the nanofluid in the presence of the Brownian diffusion and thermophoresis effects. Authors found that waviness has an essential influence on the liquid circulation and energy transport patterns.

Kasaeipoor et al. [26] investigated the energy transport of nanoliquid in a T-shaped chamber under a magnetic field influence and ascertained that the thermal transmission enhances with a growth of Richardson number and the nanoparticles concentration. Rudraiah et al. [27] examined computationally the impact of applying a constant magnetic field on the circulation of transition free convection in a square chamber with side borders of constant temperature and thermally isolated horizontal borders. They demonstrated that with increasing of magnetic field strength the convection current is lost and the heat transfer intensity is declined. Makulati et al. [28] examined the natural convection of nanofluid of water-alumina in a chamber under the influence of a magnetic field. They simulated the processes within the chamber by the conservation laws and examined the effects of Hartmann and Rayleigh numbers, nanoparticle volume fraction, chamber inclination angle, and chamber geometrical parameter. Based on their data, the thermal transmission intensity is raised with a growth of the nanoparticles concentration and the chamber inclination angle. Sidik et al. [29] analyzed the latest research on the use of hybrid nanoliquids in thermal transfer applications. They found that the thermal transfer characteristics of hybrid nanoliquids are better than the base fluids and nanofluids containing one type of nanoparticles. Sundar et al. [30] examined the improvement of convective energy transport and friction factor for the hybrid nanoliquids of multi-wall carbon nanotubes and iron oxide (III, II) in a water base fluid under the turbulent flow conditions. This research was conducted in the case of a fully developed circulation through a pipe whose surface was considered to be at a constant heat flux. The obtained data revealed that the Nusselt number for the hybrid nanoliquids was 31.1% higher than the host liquid for the Rayleigh number of 22,000. Suresh et al. [31] experimentally investigated the influence of hybrid nanofluids of copper-aluminum oxide in the water on the thermal transmission. The experiment was carried out in a tube with a circular cross-section whos surface temperature was assumed to be constant. The flow was considered at developed regime. Additionally, the pressure drop along the pipe was investigated. Overall, it was found that, for Rayleigh number of 1730, the Nusselt number increases by 13.56% relative to the base fluid. In addition, the friction factor

in hybrid nanofluids of copper-aluminum oxide/water with a volume fraction of 0.1% was clearly higher than that of the aluminum oxide/H_2O nanofluids with the same concentration of nanoparticles.

Rahimpour and Moraveji [32] examined the heat transfer of MHD free convection in a C-shaped chamber filled with Fe_3O_4/water nanofluids. They examined the impact of Hartmann and Rayleigh numbers, chamber tilted angle, nanoparticles concentration, and chamber geometrical parameter on thermal performance and fluid flow structures. In addition, they used an ANN model to model the Nusselt number and showed that the effect of Rayleigh number and chamber geometrical parameter on the thermal transmission intensity is higher than that of other variables. Islamoglu and Kurt [33] developed an ANN for analyzing heat transfer in ripple channels using experimental data. For this purpose, they used an error back propagation algorithm, which is one of the most common training algorithms in ANNs. Network inputs were the channel wave angles, the distance between the two peaks, the hydraulic diameter, and the Reynolds number and its output was the heat transfer rate. C++ programming code was also used to run the network. Finally, the accuracy of the obtained results was estimated at 4% relative to the experimental results using the mean absolute relative error. Esfe et al. [34] performed the modelling of thermal conductivity of magnesium oxide-ethylene glycol nanofluid using results from experiments and ANN. The influence of nanoparticles concentration, nanoparticles size, and temperature on the thermal conductivity of the nanofluid was measured and studied using the ANN based on the measured results. The results demonstrated that the impact of particles size and concentration of nanoparticles is higher than the influence of temperature factor on thermal conductivity of nanoparticles. Ahmadi et al. [35] modeled thermal conductivity and dynamic viscosity of Fe_2O_3/water nanoliquid using different artificial neural network techniques. Authors showed that the highest R-squared values belonged to GA-RBF (Genetic Algorithm–Radial Basis Function) method.

While different machine learning methods have been studied so far for predicting the Nusselt number, it is still unclear which method has the best performance, because the performance of each method varies depending on various factors such as the number and range of changes in the dataset and other parameters. In this research, a novel ANN-PSO network was created to model the energy transport rate. In this method, the weight and bias parameters of the ANN are optimized using the PSO algorithm and are determined in such a way that the mean squared error obtained from the observed values is less than the values predicted using the ANN. We introduce the ANN and the PSO algorithm in the following.

2. Hybrid Multi-Layer Perceptron Neural Network and Particle Swarm Optimization

2.1. Multi-Layered Artificial Neural Networks

ANNs are new computing systems and methods for machine learning, knowledge representation, and the application of the knowledge gained to model the outcomes of complicated structures. The major idea of such networks is the human brain. These systems consist of a huge number of super-interconnected processing units called neurons that operate together to define a problem and they transport information through synapses (electromagnetic coupling). An ANN includes three layers of input, output, and processing. Each layer contains a system of neurons that are generally related with neurons in other layers, but neurons of each layer are not connected to other neurons of the same layer. The neuron is the smallest data processing unit in an ANN. In this network, each neuron operates independently and the overall behavior of the network is the product of numerous neuron behaviors. Neurons correct one another in a collaborative process. Figure 1 presents the architecture of an ANN.
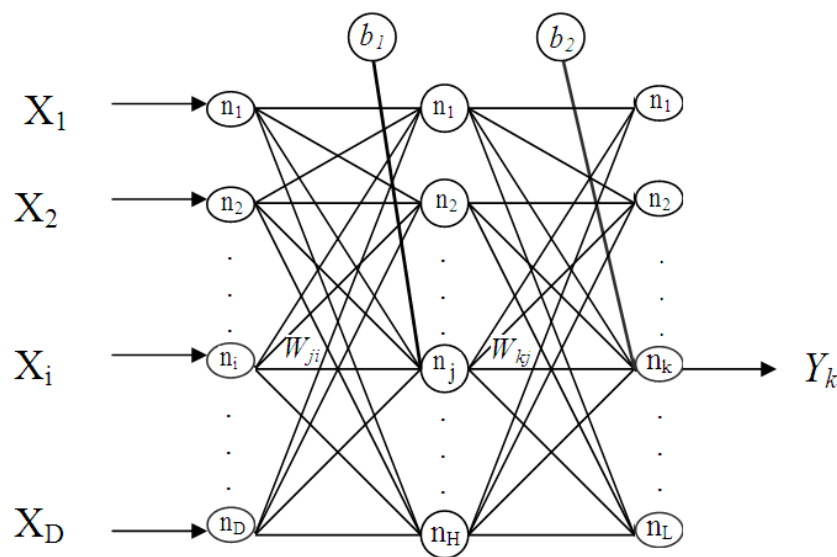
Figure 1. Typical structure of the ANN.

Neurons in the input layer only act as buffers for distributing the input signals X_i (i.e., *Ra, Ha, φ, α*, and *AR*) to neurons in the hidden layer. Each neurons *j* (Figure 1) in the hidden layer sums up its input signals X_i after weighting them with the strengths of the respective connections w_{ji} from the input layer and computes its output y_j as follow:

$$y_j = f\left(\sum_{i=1}^{D}\left(W_{ji}X_i + b_1\right)\right) \tag{1}$$

where *D* is the number of neurons in the input layer, b_1 is bias value for hidden layer, and *f* can be a simple threshold function or a sigmoid, hyperbolic tangent, or radial basis function.

During the training process these weights are adjusted to achieve optimal accuracy and coverage [36].

The training of a neural network involves the minimization of an error function. The error function for this study is defined as follows:

$$F(x) = \sum_{i=1}^{N}\left(Y_{actual,i} - Y_{predicted,i}\right)^2 \tag{2}$$

which is the same as MSE (Mean Squared Error) that should be minimized by an algorithm. *N* denotes the number of samples, while Y_{actual} and $Y_{predicted}$ are the real output (Nu_{actual}) and desired network output ($Nu_{predicted}$), respectively.

The standard method for refining a multi-layered feedforward neural network is using an error Backpropagation (BP) algorithm. During the training phase, the feedforward calculation is combined with backward error propagation to adjust the weights. Further details about BP algorithm can be found in Reference [36].

In this study, PSO is used to optimize the weights assigned to the connections between the neurons within the neural network where each particle represents a neural network with a particular set of weights. It is a "single objective" optimization which the optimization variables all arrays of the weighting matrix. The dimension of the matrix can vary as a function of ANN architecture. As all inputs and output parameters are scaled in [0, 1] so the lower and upper bounds for optimization variables are defined in the interval of (0, 1). The aim of the PSO is to find «the best weights assigned to the connections between the neurons within the neural network» producing the smallest value of the error function. The following is a brief review on PSO.

2.2. Particle Swarm Optimization (PSO)

PSO is an optimization technique based on a population of initial responses. This technique is based on the collective behavior of birds and fish species. In this method, the system starts to work with a population of initial responses and tries to find the optimal response by moving these responses during successive repetitions. The PSO algorithm shows high performance in many areas such as finding the optimal solution for functions, training ANNs, and controlling fuzzy systems. The PSO algorithm starts to work with a number of initial responses (particles) and looks for an optimal solution to the problem by moving these responses during successive repetitions. For each iteration, two values are specified: The best place in the current population (Gbest) and the place of the best value for each particle in its movement (Pbest). After finding the above values, the velocity of the particles and the next location of each particle are calculated by Equations (3) and (4), respectively.

$$V^i_{j+1} = \omega_j V^i_j + c_1 r_1 \left(W^{i,best}_j - X^i_j \right) + c_2 r_2 \left(W^{j,best}_j - X^i_j \right) \tag{3}$$

$$P^i_{j+1} = P^i_j + V^i_j \tag{4}$$

Here r_1 and r_2 are random values between 0 and 1, ω_j is the inertia weight of the jth particle, which is the effect of previous iteration on the current one, $W^{i,best}_j$ is the best value for each particle, and the parameters c_1 and c_2, also called learning coefficients, are usually equal to 2. P is referred to each particle position while V is each particle velocity. Like any other algorithm, PSO has a set of "User-Defined" parameters (i.e., Number of Particles, Maximum Number of Iterations, and inertia weight), which should be tuned by the users. There is no method for finding the best set of them except trial and error. Table 1 shows the User-Defined parameters of PSO, which has been set for this study. For more details about PSO readers are referred to [37].

Table 1. The parameters of PSO algorithm for optimizing artificial neural networks (ANNs).

Parameters	
Number of Particles	400
Iterations	240
(c_1)	2
(c_2)	2
(ω)	0.99

3. Problem Definition

We considered the natural convective energy transport in a C-shaped chamber with an inclination angle α that was filled with hybrid nanofluid [38,39]. The desired fluid is incompressible and Newtonian liquid and a two-dimensional problem was considered. The temperature of three internal borders of the chamber and two external borders of the chamber are constant with values of T_c and T_h, where T_h is greater than T_c. Additionally, two other walls are assumed to be thermally insulated and the lower border of the chamber is under variable heat flux. The length of the three internal walls of the chamber is equal to H and the length of the three outer walls of the chamber is equal to L. The chamber is also exposed to a very strong magnetic field B_0 and the acceleration of gravity g acts in negative side of y-coordinate. Figure 2 schematically presents the geometry, coordinate system, and boundary conditions for the considered problem.
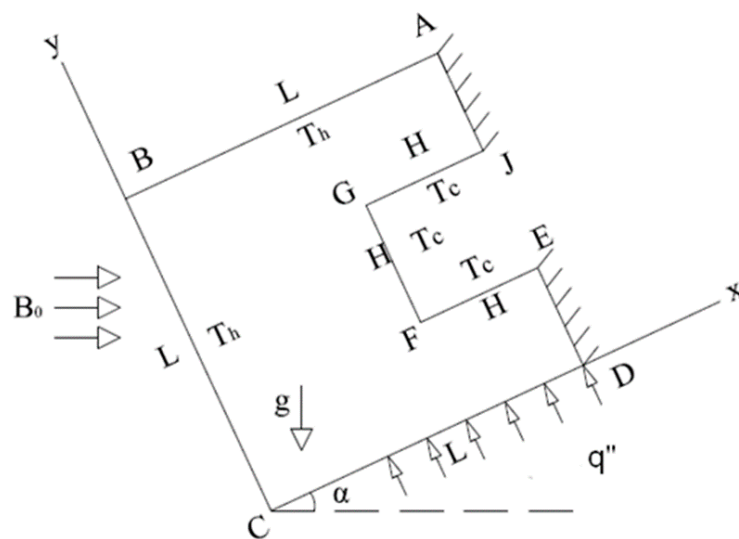
Figure 2. Sketch of the analyzed region.

4. Governing Equations

To better understand the problem, first, the governing equations of pure fluid in the closed chamber are examined. To simplify physical and mathematical equations, the following assumptions are considered:

- host liquid (pure water) and nano-sized particles Fe_3O_4-MWCNT are in thermal equilibrium;
- nanoliquid is an incompressible and Newtonian liquid;
- the liquid circulation is considered to be stable and 2D;
- thermal transmission is done by thermogravitational convection and the radiation influence is assumed negligible.
- According to these assumptions mentioned in the physical modelling, three equations of fluid conservation, namely, conservation of mass, momentum conservation in the horizontal and vertical directions, and energy conservation are shown as follows [10,14,40]:

$$\frac{\partial u}{\partial x} + \frac{\partial v}{\partial y} = 0 \tag{5}$$

$$u\frac{\partial u}{\partial x} + v\frac{\partial u}{\partial y} = -\frac{1}{\rho_{hnf}}\frac{\partial p}{\partial x} + \frac{\mu_{hnf}}{\rho_{hnf}}\left[\frac{\partial^2 u}{\partial x^2} + \frac{\partial^2 u}{\partial y^2}\right] + $$
$$+ \frac{\sigma_{hnf}}{\rho_{hnf}}B_0^2 \sin(\alpha)(v\cos(\alpha) - u\sin(\alpha)) + \frac{(\rho\beta)_{hnf}}{\rho_{hnf}}g(T - T_c)\sin(\alpha) \tag{6}$$

$$u\frac{\partial v}{\partial x} + v\frac{\partial v}{\partial y} = -\frac{1}{\rho_{hnf}}\frac{\partial p}{\partial y} + \frac{\mu_{hnf}}{\rho_{hnf}}\left[\frac{\partial^2 v}{\partial x^2} + \frac{\partial^2 v}{\partial y^2}\right] + $$
$$+ \frac{\sigma_{hnf}}{\rho_{hnf}}B_0^2 \cos(\alpha)(u\sin(\alpha) - v\cos(\alpha)) + \frac{(\rho\beta)_{hnf}}{\rho_{hnf}}g(T - T_c)\cos(\alpha) \tag{7}$$

$$u\frac{\partial T}{\partial x} + v\frac{\partial T}{\partial y} = \alpha_{hnf}\left[\frac{\partial^2 T}{\partial x^2} + \frac{\partial^2 T}{\partial y^2}\right] \tag{8}$$

where x, y, u, and v represent the horizontal and the vertical component of the location, and the velocity along the horizontal and vertical directions, respectively. Also, the temperature, pressure, density, dynamic viscosity, thermal expansion coefficient, effective electrical conductivity, magnetic field strength, gravitational acceleration, and thermal diffusivity are denoted with T, p, ρ_{hnf}, μ_{hnf}, β_{hnf}, σ_{hnf}, B_0, g, α_{hnf}, respectively.

It should be noted that the third and fourth terms in the right part of Equations (6) and (7) describe the influence of the inclined magnetic field (the third term is an inclined magnetic field effect, where

the magnetic field inclination angle is α) and inclined gravity force (the forth term characterizes an effect of the cavity inclination, where the cavity inclination angle is α).

Given the modelling problem, boundary conditions for Equations (5)–(8) are written as follows:

$T = T_h$, $u = v = 0$ on the walls of BC and AB;

$\frac{\partial T}{\partial x} = 0$, $u = v = 0$ on the walls of DE and AJ;

$T = T_c$, $u = v = 0$ on the walls of GJ, FG, and EF;

$-k_{hnf}\frac{\partial T}{\partial y} = q''$, $u = v = 0$ on the walls of CD.

The following equations are used to remove the dimension of considered control equations:

$$X = \frac{x}{L}, \; Y = \frac{y}{L}, \; U = \frac{uL}{\alpha_f}, \; V = \frac{vL}{\alpha_f}, \; AR = \frac{H}{L}, \; P = \frac{pL^2}{\rho_{hnf}\alpha_f^2}, \; \theta = \frac{T - T_c}{T_h - T_c} \tag{9}$$

The dimensionless numbers of *Ra*, Rayleigh, *Ha*, Hartmann, and *Pr*, Prandtl numbers, are defined as:

$$Ra = \frac{g\beta_f(T_h - T_c)L^3}{\nu_f\alpha_f}, \; Ha = B_0L\sqrt{\frac{\sigma_f}{\mu_f}}, \; Pr = \frac{\nu_f}{\alpha_f} \tag{10}$$

To solve the above equations, we need the thermophysical properties of the nanoliquids. Density, specific heat, volumetric expansion coefficient, and electrical conductivity were calculated through the relations presented in Table 2 [18–20,38,39].

Table 2. Thermophysical properties of the mono and hybrid nanoliquids.

Properties	Mono Nanoliquid	MWCNT-Fe$_3$O$_4$/Water
Density	$\rho_{nf} = (1-\phi)\rho_f + \phi\rho_{np}$	$(\rho C_p)_{hnf} = (1-\phi)(\rho C_p)_f + \phi_{Fe_3O_4}(\rho C_p)_{Fe_3O_4} + \phi_{MWCNT}(\rho C_p)_{MWCNT}$ $\phi = \phi_{Fe_3O_4} + \phi_{MWCNT}$
Specific heat capacity	$(\rho C_p)_{nf} = (1-\phi)(\rho C_p)_f + \phi(\rho C_p)_{np}$	$(\rho C_p)_{hnf} = (1-\phi)(\rho C_p)_f + \phi_{Fe_3O_4}(\rho C_p)_{Fe_3O_4} + \phi_{MWCNT}(\rho C_p)_{MWCNT}$
Thermal expansion coefficient	$(\rho\beta)_{nf} = (1-\phi)(\rho\beta)_f + \phi(\rho\beta)_{np}$	$(\rho\beta)_{hnf} = (1-\phi)(\rho\beta)_f + \phi_{Fe_3O_4}(\rho\beta)_{Fe_3O_4} + \phi_{MWCNT}(\rho\beta)_{MWCNT}$
Electrical conductivity	$\sigma_{nf} = \sigma_f\left(1 + \frac{3(\sigma_r-1)\phi}{(\sigma_r+2)-(\sigma_r-1)\phi}\right)$, $\sigma_r = \frac{\sigma_{np}}{\sigma_f}$	$\sigma_{hnf} = \sigma_f\left(1 + \frac{3\left(\frac{\sigma_{Fe_3O_4}}{\sigma_f}-1\right)\phi}{\left(\frac{\sigma_{Fe_3O_4}}{\sigma_f}+2\right)-\left(\frac{\sigma_{Fe_3O_4}}{\sigma_f}-1\right)\phi}\right)$

Taking into account that the value of electrical conductivity of carbon nanotube particles is order of $(O(10^{-7}))$ and it is not comparable with that of Fe$_3$O$_4$ nanoparticles where one can find the following order $(O(10^4))$. Therefore, σ_{np} is assumed to equal the electrical conductivity of ferric oxide nanoparticles.

Effective viscosity and thermal conductivity of single nanofluid (Fe$_3$O$_4$/water) are as follows [41]:

$$\mu_{nf} = \frac{\mu_f}{(1-\phi)^{2.5}}, \; \frac{k_{nf}}{k_f} = \frac{(k_{np} + 2k_f) - 2\phi(k_f - k_{np})}{(k_{np} + 2k_f) + \phi(k_f - k_{np})} \tag{11}$$

Additionally, the effective viscosity and thermal conductivity of hybrid nanofluid (MWCNT-Fe$_3$O$_4$/water) have been measured using experimental data shown in Table 3 [42].

Table 3. Effective viscosity and thermal conductivity of MWCNT-Fe$_3$O$_4$/water nanoliquid.

Volume Fraction (%)	T (°C)	k (W m^{-1}·K^{-1})	μ (mPa·s)
$\varphi = 0.0$ (host fluid)	20	0.602	0.79
	40	0.631	0.54
$\varphi = 0.1$	20	0.6734	0.91
	40	0.72	0.61
$\varphi = 0.3$	20	0.6856	1.01
	40	0.7656	0.76

After removing the dimension of Equations (5)–(8), the final form of these equations are obtained as follows:

$$\frac{\partial U}{\partial X} + \frac{\partial V}{\partial Y} = 0 \tag{12}$$

$$U\frac{\partial U}{\partial X} + V\frac{\partial U}{\partial Y} = -\frac{\partial P}{\partial X} + \frac{\mu_{nf}}{\mu_f}\frac{\rho_f}{\rho_{nf}}Pr\left[\frac{\partial^2 U}{\partial X^2} + \frac{\partial^2 U}{\partial Y^2}\right] + \frac{\sigma_{nf}}{\sigma_f}\frac{\rho_f}{\rho_{nf}}Ha^2 Pr \cdot \sin(\alpha)(V\cos(\alpha) - U\sin(\alpha)) + \\ + \frac{(\rho\beta)_{nf}}{(\rho\beta)_f}\frac{\rho_f}{\rho_{nf}}Ra \cdot Pr \cdot \theta \sin(\alpha) \tag{13}$$

$$U\frac{\partial V}{\partial X} + V\frac{\partial V}{\partial Y} = -\frac{\partial P}{\partial Y} + \frac{\mu_{nf}}{\mu_f}\frac{\rho_f}{\rho_{nf}}Pr\left[\frac{\partial^2 V}{\partial X^2} + \frac{\partial^2 V}{\partial Y^2}\right] + \frac{\sigma_{nf}}{\sigma_f}\frac{\rho_f}{\rho_{nf}}Ha^2 Pr \cos(\alpha)(U\sin(\alpha) - V\cos(\alpha)) + \\ + \frac{(\rho\beta)_{nf}}{(\rho\beta)_f}\frac{\rho_f}{\rho_{nf}}Ra \cdot Pr \cdot \theta \cos(\alpha) \tag{14}$$

$$U\frac{\partial \theta}{\partial X} + V\frac{\partial \theta}{\partial Y} = \frac{\alpha_{nf}}{\alpha_f}\left[\frac{\partial^2 \theta}{\partial X^2} + \frac{\partial^2 \theta}{\partial Y^2}\right] \tag{15}$$

The most important characteristic in energy transport is the Nusselt number. The local Nusselt number is calculated at the hot walls of the chamber, i.e., the orders AB, BC, and CD, as follows:

$$Nu_{loc} = \frac{k_{hnf}}{k_f}\left|\frac{\partial \theta}{\partial Y}\right| \text{ for borders AB and CD} \tag{16}$$

$$Nu_{loc} = \frac{k_{hnf}}{k_f}\left|\frac{\partial \theta}{\partial X}\right| \text{ for border BC} \tag{17}$$

After obtaining the local Nusselt numbers, the average Nusselt number is calculated as follows:

$$Nu = \frac{1}{3}\left(\int_B^A Nu_{loc}dX + \int_S^B Nu_{loc}dY + \int_C^D Nu_{loc}dX\right) \tag{18}$$

5. Solution of the Governing Equations

The main structure of the control equations in the present research consists of three equations of fluid conservation (conservation of mass), momentum in the horizontal and vertical directions, and the energy conservation, which are presented in the partial differential form (PDF). To solve these equations, we used computational methods and valid methods in computational fluid dynamics (CFD). In this section, a set of partial differential equations (PDEs) and corresponding boundary conditions at the walls are defined by the finite element method (FEM). FEM divides the domain of the solution into regions of elements or simple forms. In addition, in each of the simple elements, an approximate solution can be developed for a PDE. Then, a general solution is produced by interconnecting and cladding of partial solutions to ensure the continuity of the boundaries. Therefore, the PDE is satisfied in each section. The nanofluid proposed in the present study for filling the chamber is hybrid type. Therefore, the performance of the parameters such as Hartmann and Rayleigh numbers, nanoparticles concentration, and inclination angle of the chamber is investigated. The obtained data are compared

with data obtained by previous researchers and the accuracy and feasibility of the proposed model are evaluated. Also, an ANN-PSO model created in MATLAB software (2017, Math Works, Natick, MA, USA) was used to predict the heat transfer intensity as a function of the parameters mentioned and the impact of model characteristics on Nusselt number is examined and discussed. The thermal and rheological properties of the nano-sized particles and host fluid are presented in Table 4. Due to the high thermal conductivity transfer coefficient (k) of alumina (Al_2O_3), adding these nanoparticles to the fluid will have an essential influence on the increase of the total conductivity parameter of the nanofluids. The properties available from the research of Rahimpour and Moraveji [32] are shown in Table 4.

Table 4. Physicochemical properties of H_2O with Fe_3O_4 and Al_2O_3 nanoparticles.

σ ($\Omega^{-1}\cdot m^{-1}$)	β (K^{-1})	K (W m$^{-1}\cdot$K^{-1})	C (J kg$^{-1}\cdot$K^{-1})	ρ (kg$\cdot$m^{-3})	Media
0.05	2.10×10^{-4}	0.613	4179	997.1	H_2O
25,000	1.30×10^{-5}	6	670	5200	Fe_3O_4
19,900	2.17×10^{-5}	30	855	4100	Al_2O_3

6. Network Independence Analysis

The effect of meshing on the value of Nusselt numbers in different network sizes was investigated to provide that the research data are not dependent on the size of the solution network and to select the network that can ensure the validity of the results. Clearly, in a network with tighter meshing, the issue can be analyzed more accurately, but it needs more processing power to solve the problem.

Therefore, the solution grid should be chosen in such a way as to establish the equilibrium between these two important things, the accuracy of the results and the calculation burden. In order to find an appropriate network in the solving process, the Nusselt number was examined in six different standard network types. The results of examining the sizes of these networks are shown in Table 5. One can find, the Nusselt number decreases with a decrease in the size of mesh networks and it eventually remains constant. In general, the Nusselt number remains almost unchanged for the three types of Fine, Finer, and Extra Fine mesh networks. Hence, the finer mesh grid was selected. This network has 1038 domain elements and 98 border elements with high quality (see Figure 3).

Table 5. The results of examining the independence of the network in terms of φ = 0.04, *Ha* = 40, and α = 0.

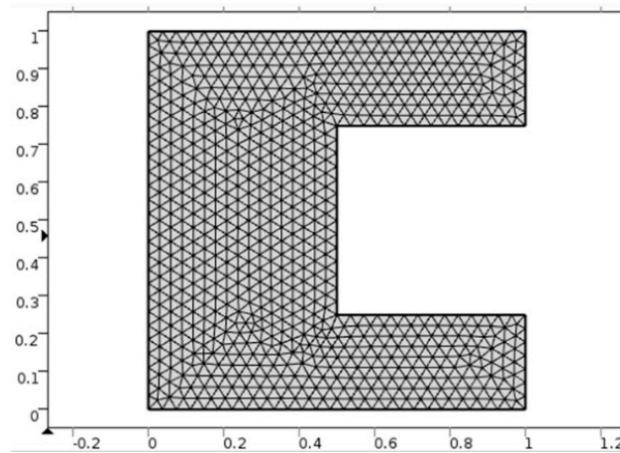| *Nu*						*Ra*	*AR*
Extra Fine	**Finer**	**Fine**	**Normal**	**Coarse**	**Coarser**		
0.87	0.87	0.87	0.87	0.88	0.88	10^2	0.2
0.092	0.092	0.092	0.093	0.093	0.094	10^4	0.2
0.243	0.243	0.244	0.245	0.246	0.248	10^6	0.2
2.53	2.53	2.53	2.54	2.54	2.55	10^2	0.05
2.65	2.65	2.66	2.67	2.68	2.60	10^4	0.05
4.73	4.75	4.76	4.77	4.79	4.81	10^6	0.05

Figure 3. Meshing the solution domain.

7. Validation of Results

To determine the accuracy and reliability of the results obtained in this study, some comparisons were made with previous studies. The results confirmed the correctness of the solution method and, as a result, validated the results of this research. For this purpose, the data were compared with data for the heat transfer of fluid inside the closed chamber under the magnetic field. Table 6 and Figure 4 demonstrate the data of the present investigation compared with those of Makulati et al. [28] and Rahimpour and Moraveji [32] on the thermal transmission of pure liquid in a closed chamber. The results are obtained in the Rayleigh number range of 10^2 to 10^6 and the constant parameters (i.e., $\varphi = 0.04$, $Ha = 0$, $AR = 0.4$, and $\alpha = 0$). The reported values are consistent with those of the mentioned studies.

Table 6. Comparison of Nusselt numbers extracted from this study and previous studies.

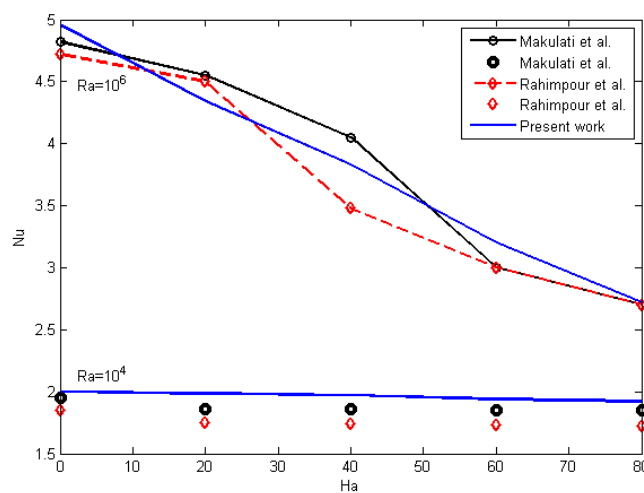| *Ra*	10^2	10^4	10^5	10^6
Makulati et al. [28]	1.882	1.952	2.654	4.823
Rahimpour and Moraveji [32]	1.875	1.853	2.634	4.721
Present study	1.922	2.115	2.853	4.966

Figure 4. Profiles of Nusselt number in comparison with References [28] and [32] at $\varphi = 0.04$, $AR = 0.4$, and $\alpha = 0$.

8. ANN Error Analysis

The accuracy of the model in the forecasting process was calculated using the correlation coefficient according to the below Equation (19), respectively. In these equations, Y_{actual} is the observed value of the function, $Y_{predicted}$ is the estimated value, and $\overline{Y}$ is the mean of the actual values. The mean squared error must be close to 0 for an optimal value and the R^2 coefficient must be maximum and close to 1.

$$R^2 = 1 - \frac{\sum\limits_{i=1}^{N}\left(Y_{actual,i} - Y_{predicted,i}\right)^2}{\sum\limits_{i=1}^{N}\left(Y_{actual,i} - \overline{Y}\right)^2} \tag{19}$$

The results of comparing the output obtained from the ANN and the ANN-PSO show that the optimization algorithm partially improved the results of ANN. The SME values of the ANN and ANN-PSO models are 0.35 and 0.22, respectively. Figure 5 presents the linear regression between actual outputs and ANN outputs optimized for training data sets. This figure displays the prediction of network based on input data and compares it with the real data. The dispersion of the values predicted for the Nusselt number shows a close relationship between the CFD results and the results obtained in the ANN-PSO. Regarding the correlation coefficient $R^2 = 0.999$, the error value is minimal. In this method, the Nusselt number was predicted accurately using an optimized ANN, indicating its high ability to provide reliable predictions.
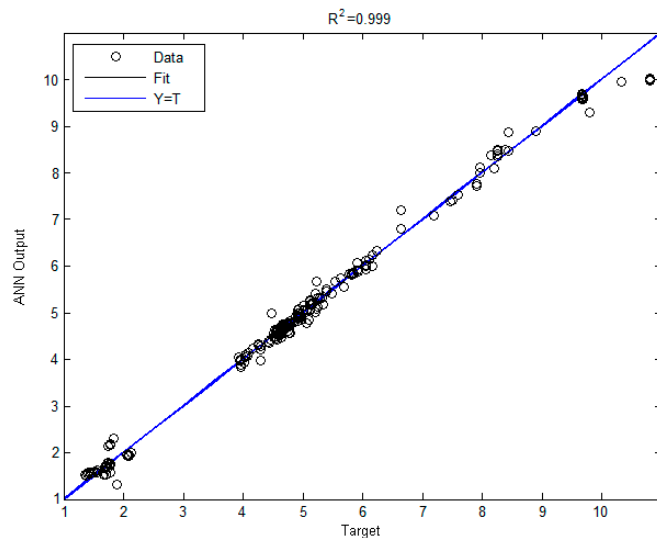

Figure 5. Dispersion of ANN-PSO outputs compared to Computational Fluid Dynamics (CFD) outputs.

9. Results and Discussion

In this section, the results of the obtained governing equations are presented in the form of charts and tables. Initially, the heat transfer within a chamber was modeled using COMSOL software and the Nusselt number was obtained using output data.

The magnetic field has an essential influence on the motion field and temperature due to the Lorentz force. The impact of the magnetic field on the energy transport intensity has been investigated in the form of Hartmann number change in the range of $0 \le Ha \le 80$. For this purpose, other parameters are considered constant (i.e., $\varphi = 0.05$, $AR = 0.5$, and $\alpha = 0$). At the same time, the effect of gravity force in the case of vertical cavity is significant taking into account the presence of heat sources and heat sinks with constant high and low temperatures. This influence is described by the Rayleigh number variation.

As presented in Figure 6, the ANN-PSO data are in good agreement with the values obtained using the CFD. For Rayleigh number values between 10^2 and 10^4, the variation of *Nu* with growing of *Ha* is negligible and almost is constant. It can also be seen that for higher Rayleigh number values, *Nu* reduces linearly with a rising of *Ha* and a large drop in *Nu* occurs, especially for *Ha* that is equal to 80, which is due to Lorentz force overlying the flotation by increasing the magnetic field. Figure 7 shows the dependency of *Nu* on the chamber inclination angle. For this purpose, other parameters are considered constant (i.e., $\varphi = 0.05$, $Ha = 0$, and $Ra = 10^6$). According to the curves of Figure 7, *Nu* enhances with a raise of the chamber tilted angle. However, for smaller aspect ratios (*AR*), the increment of *Nu* is greater with rising of the inclination angle of the chamber. Here, the highest Nusselt number value was also recorded at a chamber inclination angle of 90°. Figure 8 presents the effect of changes of nanoparticles concetration, flow behavior for various Rayleigh numbers, and φ changes in the range of $0 \leq \varphi \leq 0.1$. Comparison of the curves of this figure demonstrates that with the increasing of the nano-sized particles concentration, the Nusselt number increases for low and high Rayleigh numbers and the increase level in the lower Rayleigh numbers is higher, especially for Rayleigh number of 10^4. According to the obtained results, it can be concluded that the increase in nanoparticles concentration raises the conductivity of the hybrid nanoliquid and thus enhances the energy transport.
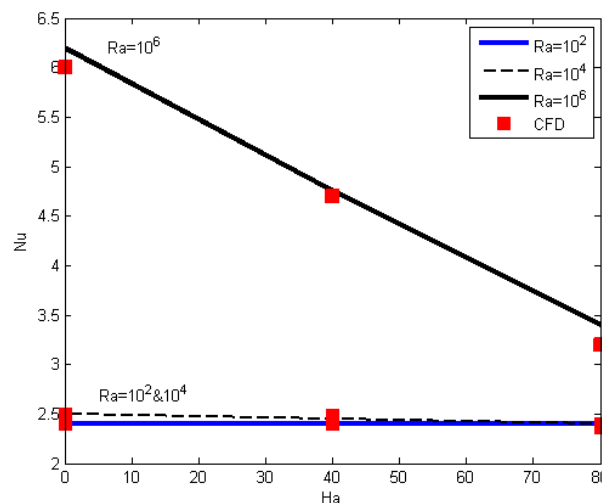

Figure 6. Examining the Nusselt number relative to the Hartmann number at $\varphi = 0.05$, $AR = 0.5$, and $\alpha = 0$.
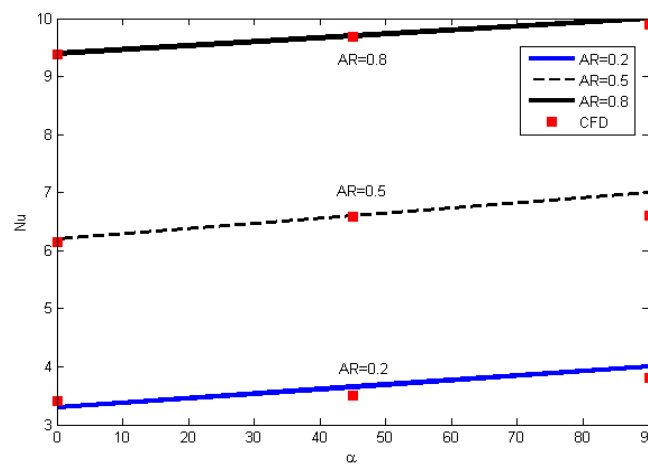

Figure 7. Examining the Nusselt number relative to the angle of the chamber at $\varphi = 0.05$, $Ha = 0$, and $Ra = 10^6$.
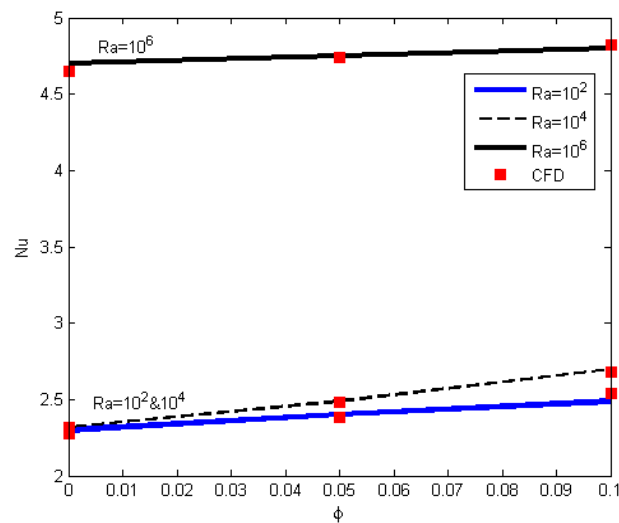
Figure 8. The Nusselt number survey relative to the volume of nanoparticles at *Ha* = 40, *AR* = 0.5, and α = 0.

In order to provide the quality of the results obtained by the hybrid nanoliquid, and also to demonstrate the great effect of using hybrid nanoliquid compared to the mono nanofluid, two types of nanofluids Fe_3O_4/H_2O and Al_2O_3/H_2O relative to hybrid nanofluid $MWCNT$-Fe_3O_4/H_2O were studied at constant operating conditions and the same geometry. In all three studies, the parameters are considered constant (i.e., φ = 0.05, *Ha* = 0, *AR* = 0.5, and α = 0). According to Figure 9, the highest Nusselt number is obtained for hybrid nanofluid at both low and high Rayleigh numbers. Especially, Nusselt number was recorded 6.2 for Rayleigh number of 10^6, indicating the superiority of the hybrid nanofluid to nanofluid.
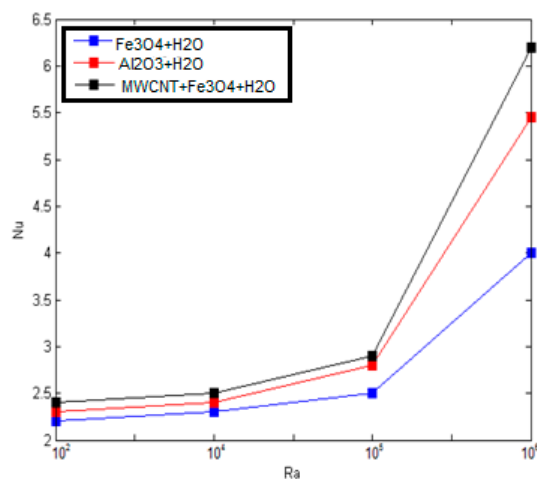

Figure 9. The Nusselt number survey relative to the Rayleigh number for three different nanofluids at φ = 0.05, *Ha* = 0, *AR* = 0.5, and α = 0.

10. Conclusions

In this research, the thermogravitational convection was investigated in a C-shaped chamber with an angle of gravity α that was filled with a hybrid nanoliquid under the influence of magnetic field and thermal flux. Then, the impacts of Rayleigh number ($10^2 \leq Ra \leq 10^6$), Hartmann number ($0 \leq Ha \leq 80$), nanoparticles concentration ($0 \leq \varphi \leq 0.1$), chamber inclination angle ($0 \leq \alpha \leq \pi/2$), and aspect ratio ($0.05 \leq AR \leq 0.8$) were investigated on Nusselt number. Afterward, using the ANN combined with the

PSO technique, the Nusselt number was predicted and investigated against the parameters mentioned. Overall, the results of this study can be summarized as follows:

- The results obtained from the analysis of the Nusselt number by the ANN-PSO are in good harmony with the Nusselt obtained in CFD, suggesting the prediction accuracy of the optimal ANN.
- The mean squared error in the ANN and ANN-PSO models was 0.35 and 0.22, respectively, indicating the accuracy of the latter.
- The impact of five variables on *Nu* was investigated that among the variables studied. *Ra* and *AR* had the greatest effect on *Nu* so that *Nu* was increased with a growth of *Ra* and *AR*. Additionally, the data showed that increasing the Hartmann number for high *Ra* reduced the Nusselt number, while the changes in the Hartmann number did not significantly affect *Nu* for *Ra* between 10^4 and 10^6.
- According to the results obtained, the use of a hybrid nanofluid instead of a mono nanofluid increases the heat transfer coefficient so that the Nusselt number increases in both low and high Rayleigh values.

Conflicts of Interest: The authors declare no conflict of interest.

Abbreviations

The following abbreviations are used in this manuscript:

AR	aspect ratio
b_1	bias value for hidden layer
B_0	magnetic field strength (T)
c_1, c_2	particle's learning coefficients
C_p	specific heat at constant pressure (J/kg·K)
D	number of neurons
f	threshold function
F(X)	error function
g	gravitational acceleration (m/s^2)
H	internal length of cavity (m)
Ha	Hartmann number
k	thermal conductivity (W/m·K)
L	external length of cavity (m)
Nu	Nusselt number
p	dimensional fluid pressure (Pa)
P	dimensionless pressure
P_i^j	particle position
Pr	Prandtl number
q''	heat flux at the bottom wall
R^2	correlation coefficient
Ra	Rayleigh number
T	temperature (K)
u, v	dimensional velocity components in the *x, y* directions (m/s)
U, V	dimensionless velocity components
V_i^j	particle velocity

w	network weighting parameters
$W_j^{i,best}$	particle's best position
x, y	Cartesian coordinates (m)
X, Y	dimensionless coordinates
X_i	neurons in the input layer
Y_{actual}	real output
$Y_{predicted}$	predicted output
$\overline{Y}$	mean of the actual values

Greek symbols

α	inclination angle (deg)
α_f	thermal diffusivity (m^2/s)
β	thermal expansion coefficient (1/K)
φ	nanoparticles volume fraction
σ	effective electrical conductivity (1/X·m)
θ	dimensionless temperature
ν_f	kinematic viscosity (m^2/s)
ρ	density (kg/m^3)
μ	viscosity (mPa·s)
ω	inertia weight

Subscripts

f	base fluid
loc	local
nf	nanofluid
np	nanoparticles

References

1. Choi, S.U.S. Enhancing thermal conductivity of fluids with nanoparticles. In *Developments Applications of Non-NewtonianFlows*; ASME: San Francisco, CA, USA, 1995; Volume 231, pp. 99–105.
2. Izadi, M.; Shahmardan, M.M.; Behzadmehr, A. Richardson number ratio effect on laminar mixed convection of a nanofluid flow in an annulus. *Int. J. Comput. Methods Eng. Sci. Mech.* **2013**, *14*, 304–316. [CrossRef]
3. Izadi, M.; Behzadmehr, A.; Shahmardan, M.M. Effects of inclination angle on laminar mixed convection of a nanofluid flowing through an annulus. *Chem. Eng. Commun.* **2015**, *202*, 1693–1702. [CrossRef]
4. Izadi, M.; Behzadmehr, A.; Shahmardan, M.M. Effects of inclination angle on mixed convection heat transfer of a nanofluid in a square cavity. *Int. J. Comput. Methods Eng. Sci. Mech.* **2015**, *16*, 11–21. [CrossRef]
5. Izadi, M.; Shahmardan, M.M.; Norouzi, M.; Rashidi, A.M.; Behzadmehr, A. Cooling performance of a nanofluid flow in a heat sink microchannel with axial conduction effect. *Appl. Phys. A Mater. Sci. Process.* **2014**, *117*, 1821–1833. [CrossRef]
6. Izadi, M.; Mohebbi, R.; Chamkha, A.; Pop, I. Effects of cavity and heat source aspect ratios on natural convection of a nanofluid in a C-shaped cavity using Lattice Boltzmann method. *Int. J. Numer. Methods Heat Fluid Flow* **2018**, *28*, 1930–1955. [CrossRef]
7. Mehryan, S.; Ghalambaz, M.; Izadi, M. Conjugate natural convection of nanofluids inside an enclosure filled by three layers of solid, porous medium and free nanofluid using Buongiorno's and local thermal non-equilibrium models. *J. Therm. Anal. Calorim.* **2019**, *135*, 1047–1067. [CrossRef]
8. Mohebbi, R.; Izadi, M.; Delouei, A.A.; Sajjadi, H. Effect of MWCNT–Fe$_3$O$_4$/water hybrid nanofluid on the thermal performance of ribbed channel with apart sections of heating and cooling. *J. Therm. Anal. Calorim.* **2019**, *135*, 3029–3042. [CrossRef]
9. Izadi, M.; Sinaei, S.; Mehryan, S.; Oztop, H.F.; Abu-Hamdeh, N. Natural convection of a nanofluid between two eccentric cylinders saturated by porous material: Buongiorno's two phase model. *Int. J. Heat Mass Transf.* **2018**, *127*, 67–75. [CrossRef]
10. Mehryan, S.; Izadi, M.; Chamkha, A.J.; Sheremet, M.A. Natural convection and entropy generation of a ferrofluid in a square enclosure under the effect of a horizontal periodic magnetic field. *J. Mol. Liq.* **2018**, *263*, 510–525. [CrossRef]

11. Izadi, M.; Mohebbi, R.; Delouei, A.A.; Sajjadi, H. Natural convection of a magnetizable hybrid nanofluid inside a porous enclosure subjected to two variable magnetic fields. *Int. J. Mech. Sci.* **2019**, *151*, 154–169. [CrossRef]

12. Izadi, M.; Mehryan, S.; Sheremet, M.A. Natural convection of CuO-water micropolar nanofluids inside a porous enclosure using local thermal non-equilibrium condition. *J. Taiwan Inst. Chem. Eng.* **2018**, *88*, 89–103. [CrossRef]

13. Sajjadi, H.; Delouei, A.A.; Izadi, M.; Mohebbi, R. Investigation of MHD natural convection in a porous media by double MRT lattice Boltzmann method utilizing MWCNT–Fe_3O_4/water hybrid nanofluid. *Int. J. Heat Mass Transf.* **2019**, *132*, 1087–1104. [CrossRef]

14. Mehryan, S.; Sheremet, M.A.; Soltani, M.; Izadi, M. Natural convection of magnetic hybrid nanofluid inside a double-porous medium using two-equation energy model. *J. Mol. Liq.* **2019**, *277*, 959–970. [CrossRef]

15. Izadi, M.; Pour, S.H.; Yasuri, A.K.; Chamkha, A.J. Mixed convection of a nanofluid in a three-dimensional channel: Effect of opposed buoyancy force on hydrodynamic parameters, thermal parameters and entropy generation. *J. Therm. Anal. Calorim.* **2019**, *136*, 2461–2475. [CrossRef]

16. Izadi, M.; Maleki, N.M.; Pop, I.; Mehryan, S. Natural convection of a hybrid nanofluid subjected to non-uniform magnetic field within porous medium including circular heater. *Int. J. Numer. Methods Heat Fluid Flow* **2019**, *29*, 1211–1231. [CrossRef]

17. Izadi, M.; Javanahram, M.; Zadeh, S.M.H.; Jing, D. Hydrodynamic and heat transfer properties of magnetic fluid in porous medium considering nanoparticle shapes and magnetic field-dependent viscosity. *Chin. J. Chem. Eng.* **2019**. [CrossRef]

18. Sajid, M.U.; Ali, H.M. Recent advances in application of nanofluids in heat transfer devices: A critical review. *Renew. Sustain. Energy Rev.* **2019**, *103*, 556–592. [CrossRef]

19. Assael, M.J.; Antoniadis, K.D.; Wakeham, W.A.; Zhang, X. Potential applications of nanofluids for heat transfer. *Int. J. Heat Mass Transf.* **2019**, *138*, 597–607. [CrossRef]

20. Huminic, G.; Huminic, A. Hybrid nanofluids for heat transfer applications—A state-of-the-art review. *Int. J. Heat Mass Transf.* **2018**, *125*, 82–103. [CrossRef]

21. Khanafer, K.; Vafai, K.; Lightstone, M. Buoyancy-Driven heat transfer enhancement in a two-dimensional enclosure utilizing nanofluids. *Int. J. Heat Mass Transf.* **2003**, *46*, 3639–3653. [CrossRef]

22. Ganvir, R.B.; Walke, P.V.; Kriplani, V.M. Heat transfer characteristics in nanofluid—A review. *Renew. Sustain. Energy Rev.* **2017**, *75*, 451–460. [CrossRef]

23. Kalidasan, K.; Rajesh Kanna, P. Effective utilization of MWCNT-water nanofluid for enhancement of laminar natural convection inside the open square enclosure. *J. Taiwan Inst. Chem. Eng.* **2016**, *65*, 331–340. [CrossRef]

24. Hasanuzzaman, M.; Oztop, H.F.; Rahman, M.M.; Rahim, N.A.; Saidur, R.; Varol, Y. Magnetohydrodynamic natural convection in trapezoidal cavities. *Int. Commun. Heat Mass Transf.* **2012**, *39*, 1384–1394. [CrossRef]

25. Sheremet, M.A.; Cimpean, D.S.; Pop, I. Free convection in a partially heated wavy porous cavity filled with a nanofluid under the effects of Brownian diffusion and thermophoresis. *Appl. Therm. Eng.* **2017**, *113*, 413–418. [CrossRef]

26. Kasaeipoor, A.; Ghasemi, B.; Aminossadati, S.M. Convection of Cu-water nanofluid in a vented T-shaped cavity in the presence of magnetic field. *Int. J. Therm. Sci.* **2015**, *94*, 50–60. [CrossRef]

27. Rudraiah, N.; Barron, R.M.; Venkatachalappa, M.; Subbaraya, C.K. Effect of a magnetic field on free convection in a rectangular enclosure. *Int. J. Eng. Sci.* **1995**, *33*, 1075–1084. [CrossRef]

28. Makulati, N.; Kasaeipoor, A.; Rashidi, M.M. Numerical study of natural convection of a water–alumina nanofluid in inclined C-shaped enclosures under the effect of magnetic field. *Adv. Powder Technol.* **2016**, *27*, 661–672. [CrossRef]

29. Sidik, N.A.C.; Adamu, I.M.; Jamil, M.M.; Kefayati, G.H.R.; Mamat, R.; Najafi, G. Recent progress on hybrid nanofluids in heat transfer applications: A comprehensive review. *Int. Commun. Heat Mass Transf.* **2016**, *78*, 68–79. [CrossRef]

30. Sundar, L.S.; Singh, M.K.; Sousa, A.C.M. Enhanced heat transfer and friction factor of MWCNT–Fe_3O_4/water hybrid nanofluids. *Int. Commun. Heat Mass Transf.* **2014**, *52*, 73–83. [CrossRef]

31. Suresh, S.; Venkitaraj, K.P.; Selvakumar, P.; Chandrasekar, M. Effect of Al_2O_3-Cu/water hybrid nanofluid in heat transfer. *Exp. Therm. Fluid Sci.* **2012**, *38*, 54–60. [CrossRef]

32. Rahimpour, N.; Moraveji, M.K. Free convection of water–Fe_3O_4 nanofluid in an inclined cavity subjected to a magnetic field: CFD modeling, sensitivity analysis. *Adv. Powder Technol.* **2017**, *28*, 1573–1584. [CrossRef]

33. Islamoglu, Y.; Kurt, A. Heat transfer analysis using ANNs with experimental data for air flowing in corrugated channels. *Int. J. Heat Mass Transf.* **2004**, *47*, 1361–1365. [CrossRef]

34. Esfe, M.H.; Saedodin, S.; Bahiraei, M.; Toghraie, D.; Mahian, O.; Wongwises, S. Thermal conductivity modeling of MgO/EG nanofluids using experimental data and artificial neural network. *J. Therm. Anal. Calorim.* **2014**, *118*, 287–294. [CrossRef]

35. Ahmadi, M.H.; Tatar, A.; Seifaddini, P.; Ghazvini, M.; Ghasempour, R.; Sheremet, M.A. Thermal conductivity and dynamic viscosity modeling of Fe_2O_3/water nanofluid by applying various connectionist approaches. *Numer. Heat Transf. A* **2018**, *74*, 1301–1322. [CrossRef]

36. Pham, D.T.; Liu, X. *Neural Networks for Identification, Prediction and Control*; Springer: Berlin, Germany, 1995.

37. Assareh, E.; Behrang, M.A.; Assari, M.R.; Ghanbarzadeh, A. Application of PSO (particle swarm optimization) and GA (genetic algorithm) techniques on demand estimation of oil in Iran. *Energy* **2010**, *35*, 5223–5229. [CrossRef]

38. Siddiqui, F.R.; Tso, C.Y.; Chan, K.C.; Fu, S.C.; Chao, C.Y.H. On trade-off for dispersion stability and thermal transport of Cu-Al_2O_3 hybrid nanofluid for various mixing ratios. *Int. J. Heat Mass Transf.* **2019**, *132*, 1200–1216. [CrossRef]

39. Babu, J.A.R.; Kumar, K.K.; Rao, S.S. State-of-art review on hybrid nanofluids. *Renew. Sustain. Energy Rev.* **2017**, *77*, 551–565. [CrossRef]

40. Armaghani, T.; Kasaeipoor, A.; Izadi, M.; Pop, I. MHD natural convection and entropy analysis of a nanofluid inside T-shaped baffled enclosure. *Int. J. Numer. Methods Heat Fluid Flow* **2018**, *28*, 2916–2941. [CrossRef]

41. Brinkman, H.C. The viscosity of concentrated suspensions and solutions. *J. Chem. Phys.* **1952**, *20*, 571. [CrossRef]

42. Sundar, L.S.; Sousa, A.C.M.; Singh, M.K. Heat transfer enhancement of low volume concentration of carbon nanotube-Fe_3O_4/water hybrid nanofluids in a tube with twisted tape inserts under turbulent flow. *J. Therm. Sci. Eng. Appl.* **2015**, *7*, 021015. [CrossRef]